Arch Appl Mech (2017) 87:853–864
DOI 10.1007/s00419-016-1183-z

SPECIAL

Valter Böhm · Tobias Kaufhold · Igor Zeidis · Klaus Zimmermann

Dynamic analysis of a spherical mobile robot based on a tensegrity structure with two curved compressed members

Received: 16 March 2016 / Accepted: 10 September 2016 / Published online: 13 October 2016

Abstract The use of mechanically compliant tensegrity structures in mobile robotics is an attractive research topic. The mechanical properties and therefore the locomotion performance of mobile robots based on these structures can be adjusted reversibly during locomotion. In the present work, a rolling mobile robot, based on a simple tensegrity structure, consisting of two rigid disconnected curved members connected to a continuous net of eight prestressed tensioned members with pronounced elasticity, is considered. Pure rolling uniaxial locomotion and also planar locomotion can be realized with small control effort, induced by the movement of two internal masses. After kinematic considerations, the nonlinear equations of motion are derived and transient dynamic analyses are performed, to study the system behavior. Also the dependency of the rolling movement behavior on structural and actuation parameters is discussed. The uniaxial and planar locomotion performance of the system are verified experimentally.

Keywords Tensegrity structure · Mobile robot · Rolling locomotion · Internal mass movement · Dynamic analysis

1 Introduction

The use of mechanically prestressed compliant structures in mobile robotics is a recently discussed topic. One specific class of these structures build tensegrity structures, consisting of a set of rigid disconnected compressed members connected to a continuous net of prestressed tensioned members. Robots based on these structures are deployable, lightweight, have a simple system design, very high strength to weight ratio, and shock absorbing capabilities [1–3]. An overview of actual developments and development directions can be found in [4–8]. A recent development direction is the realization of rolling mobile robots based on these structures [9–11]. Known systems use conventional tensegrity structures, based on straight members. Locomotion is realized by body deformation and tip-over movement sequences, due to periodically changing the length of selected tensioned or compressed members. The future realization of pure rolling locomotion ("smooth rolling") with these robots is only possible with large control effort.

The application of curved members in tensegrity structures indicates their potential ability for the use in rolling mobile robots. In the present work, the authors focus on the dynamic properties of a simple rolling mobile robot, based on a spatial non-conventional tensegrity structure with two curved compressed members. The actuation of the system is based on internal mass movement, to minimize the control effort. Locomotion of the robot is possible without body deformation. Selected properties of the considered system are introduced in [12]. In the present contribution, a more detailed analysis of the system's kinematics and also an experimental study is presented, to verify the theoretical results. In Sect. 2, the structure, the assumptions, and the type of

V. Böhm (✉) · T. Kaufhold · I. Zeidis · K. Zimmermann
Technical Mechanics Group, Ilmenau University of Technology, 98693 Ilmenau, Germany
E-mail: valter.boehm@tu-ilmenau.de

actuation of the system are discussed. After considerations on the system's kinematics in Sect. 3, with the help of a simple equivalent mechanical model, basic dynamic properties of the system and experimental results are presented in Sect. 4.

2 Structural properties, assumptions, and type of actuation

The considered tensegrity structure, based on [13], consists of two equal curved members (j=0,1) with constant radius of curvature R and length $R\pi$ (Fig. 1a). The curved bended members (called as compressed, due to the tensegrity terminology) are indirectly interconnected through eight tensioned members. Each end point of one curved member is connected with both end points of the other curved member (four tensioned members of type 1 between 00–10, 00–11, 01–10, and 01–11, initial length L_{01}, longitudinal stiffness k_1). Furthermore, the points 02 at φ_0=0 and 12 at $\varphi_1 = 0$ are connected with the end points of the other compressed member (4 tensioned members of type 2 between 02-10, 02-11, 12-00, and 12-01, initial length L_{02}, longitudinal stiffness k_2). The structure is in the symmetrical configuration, as depicted in Fig. 1a, in stable equilibrium (curved member 0 with the points 00, 01 and 02 in the $x_0 - y_0$ plane, curved member 1 with the connecting points 10, 11 and 12 in the y_0-z_0 plane; with equal deformed lengths for both types of tensioned members L_1 and L_2, where $L_1 \neq L_2$). The shape of the structure in this configuration is defined by the parameters of the tensioned members and can be expressed only by the parameters d (distance between the arc center points) and R. Considering the equilibrium, the location vectors of the attachment points between the tensioned and compressed members and the parameter d can be found (j=0,1; i=0,1,2)

$$\vec{r}_{\mathrm{ji}} = R \cdot \{(1-j)(1-i/2)(1-3i),\ (j-1/2)\,(i(i-1)-d/R)\,,\ j(1-i/2)(1-3i)\}^{\mathrm{T}}, \quad \frac{d/R}{1-d/R} = \frac{k_2(1-L_{02}/L_2)}{k_1(1-L_{01}/L_1)}. \tag{1}$$

The locomotion system based on the introduced structure is capable of uniaxial rolling and also of planar movement with combined tip-over and rolling [12,14,15] (see Fig. 1e). To realize locomotion, two equal internal masses are moved along lines connecting the end points of the curved members with two linear stepping motors (Fig. 1d).

The rolling movement consists of several repeated basic movement sequences. During a sequence, the robot has at two points contact to the ground: a non-changing endpoint of a curved compressed member, and a continuously changing second point on the other curved compressed member. At the end of each moving sequence, the continuously changing second contact point reaches an end point and then changes to a non-changing contact point. At the subsequent rolling sequence, the process repeats with a change between the curved members, with respect to which a rolling movement occurs.

Following assumptions are used in the theoretical considerations:

- The internally moved masses are considered as mass points (A_0 and A_1, where $m_{A0} = m_{A1} = m$), masses and mass moments of inertia of other system parts are neglected. The time-dependent position $a_j(t)$ of mass point A_j is given with the relative distance from the end point $j1$ of member j.
- The prestress of the system is assumed as high. Elastic deformations of the system, due to gravitational and dynamic forces, are neglected. Therefore, the mechanical compliance of the system is small, but the system is able to absorb shocks (e.g. falling) and is foldable (advantageous by transportation in space applications).
- The gravity vector is perpendicular to the plane ($\vec{g} = -g \cdot \vec{e}_z = -9810mm/s^2 \cdot \vec{e}_z$).

3 Kinematics of the system

To describe the system's kinematics for a basic movement sequence, corresponding to rolling on one curved member, rolling motion of a rigid circular disc (radius a) on a plane ground surface (x-y plane) without slipping is considered (Figs. 1c, 2). On the disc (center: point C) a rigid rod with end points O, N is eccentrically connected normal to the disc plane (connection point N), without relative movement capability between disc and rod. The free end of the rod (point O) is rotatable supported in the origin of the inertial coordinate system.

The position of the contact point K ($\vec{r} = \vec{\mathrm{OK}} = x\vec{e}_x + y\vec{e}_y$) between disc and ground is to be determined in dependence on the rotation angle φ. The coordinates of the position vector $\vec{r}$ are

$$x = r\cos(\psi+\beta) \quad \text{and} \quad y = r\sin(\psi+\beta), \tag{2}$$

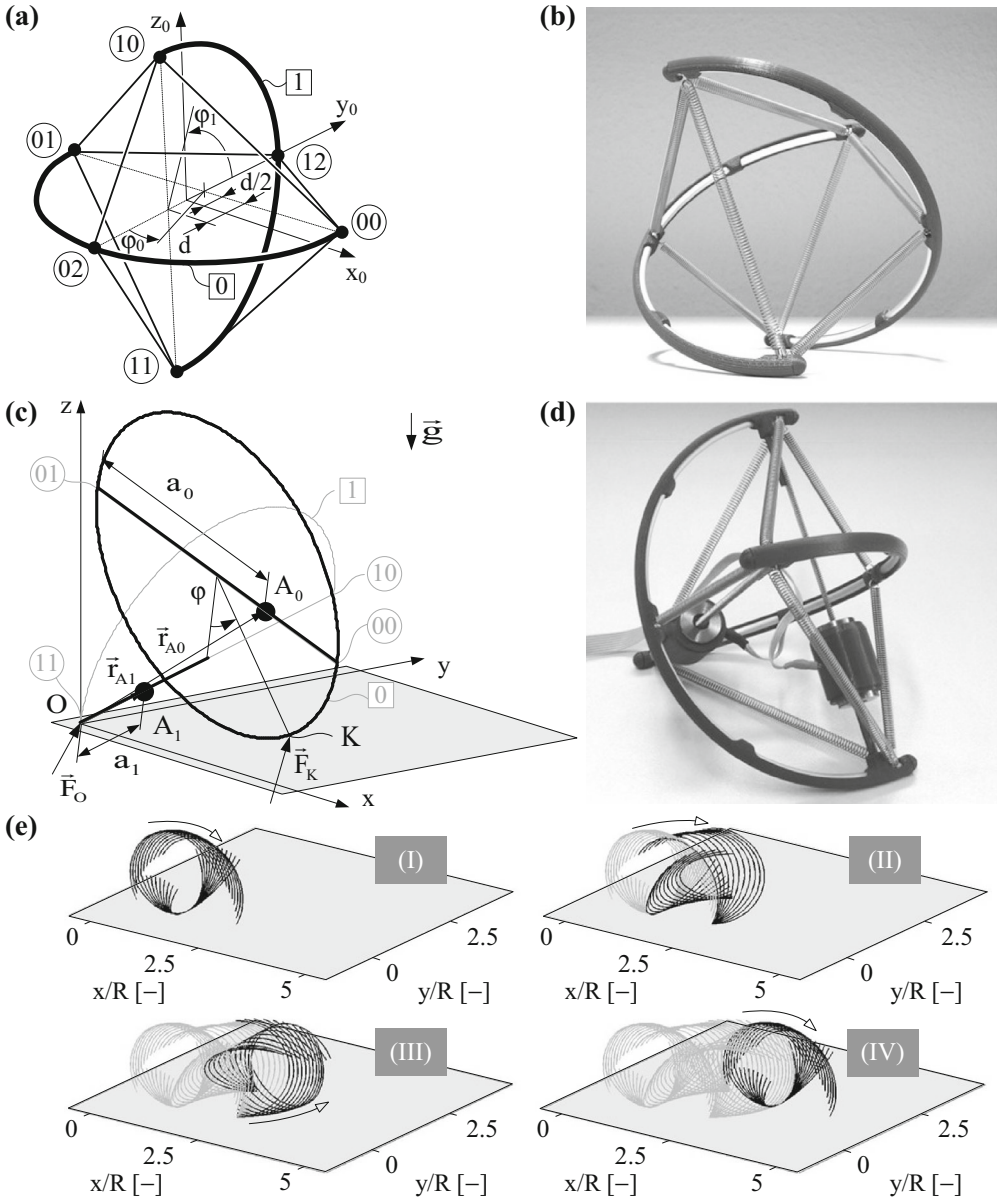

Fig. 1 Mechanical model (**a**) of the tensegrity structure (**b**), and mechanical model (**c**) of the considered corresponding locomotion system (**d**), and a possible locomotion sequence (**e**) ((I)→(IV); (I),(IV): tip-over; (II),(III): rolling-basic movement sequence, displaying only the curved compressed members)

where $r = |\vec{r}| = (x^2 + y^2)^{0.5}$. The goal is to determine the coordinates of the position vector as a function of φ. Therefore, the relationship between the angles $\psi + \beta$ and φ is to be determined. Using the geometrical relationships (see Fig. 2)

$$x^2 + y^2 = L^2/\cos^2\theta + d^2\sin^2\varphi \text{ and } a - d\cos\varphi = L\tan\theta, \tag{3}$$

the following relationship between x, y, and the rotation angle φ can be found

$$x^2 + y^2 = L^2 + a^2 + d^2 - 2ad\cos\varphi. \tag{4}$$

In accordance with (2) the coordinates of the velocity vector $\dot{\vec{r}} = \dot{x}\vec{e}_x + \dot{y}\vec{e}_y$ are

$$\dot{x} = \dot{r}cos(\psi+\beta) - rsin(\psi+\beta)(\dot{\psi}+\dot{\beta}) \text{ and } \dot{y} = \dot{r}sin(\psi+\beta) + rcos(\psi+\beta)(\dot{\psi}+\dot{\beta}). \tag{5}$$

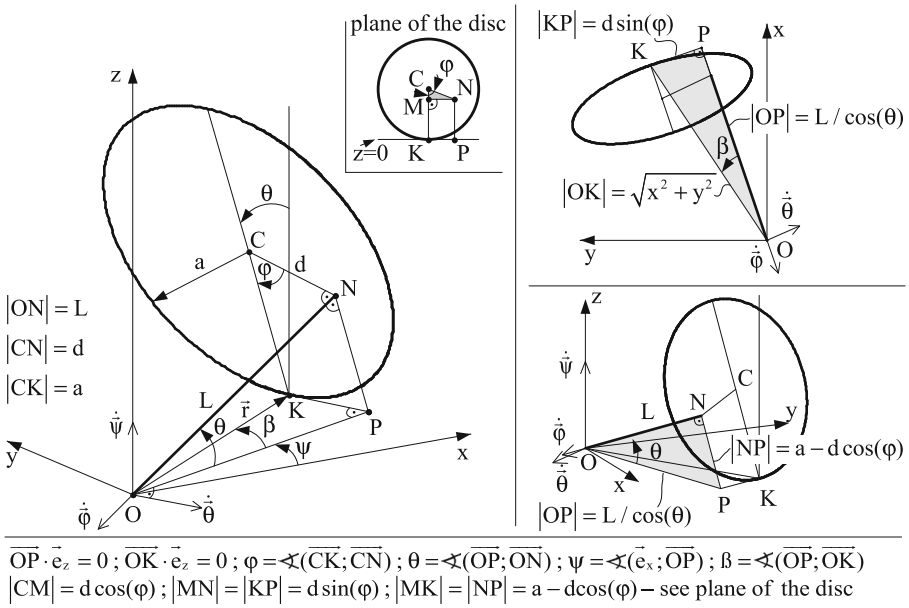

Fig. 2 The considered mechanical model with geometric parameters in different views (important geometric relationships are marked with gray right-angled triangles; $0 \leq d < a$)

These coordinates can also be expressed with the help of the classical condition for rolling without slipping

$$\dot{x} = -a\dot{\varphi}\sin\psi \text{ and } \dot{y} = a\dot{\varphi}\cos\psi. \tag{6}$$

From (5) and (6) follows

$$\dot{r}\cos(\psi+\beta) - r\sin(\psi+\beta)(\dot{\psi}+\dot{\beta}) = -a\dot{\varphi}\sin\psi \text{ and } \dot{r}\sin(\psi+\beta) + r\cos(\psi+\beta)(\dot{\psi}+\dot{\beta}) = a\dot{\varphi}\cos\psi. \tag{7}$$

The transformation of equations (7) leads to

$$r(\dot{\psi}+\dot{\beta}) = a\dot{\varphi}\,(\sin\psi\sin(\psi+\beta) + \cos\psi\cos(\psi+\beta)) = a\dot{\varphi}\cos\beta. \tag{8}$$

With regard to the geometric relationships $\cos\theta = L/(L^2 + (a - d\cos\varphi)^2)^{0.5}$ and $\cos\beta = L/(r\cos\theta)$ (see gray triangles in Fig. 2) from (8) follows the direct relationship between the angles $(\psi+\beta)$ and φ

$$\dot{\psi}+\dot{\beta} = \dot{\varphi}a(L^2 + (a - d\cos\varphi)^2)^{0.5}(L^2 + a^2 + d^2 - 2ad\cos\varphi)^{-1}, \tag{9}$$

$$\psi+\beta = \int_0^{\varphi} a(L^2 + (a - d\cos\xi)^2)^{0.5}(L^2 + a^2 + d^2 - 2ad\cos\xi)^{-1}d\xi. \tag{10}$$

In summary, the coordinates x, y, and the angles θ and ψ in dependence on the rotation angle φ are

$$x = (L^2 + a^2 + d^2 - 2ad\cos\varphi)^{0.5}\cos\left(\int_0^{\varphi}\frac{a(L^2 + (a - d\cos\xi)^2)^{0.5}}{L^2 + a^2 + d^2 - 2ad\cos\xi}d\xi\right), \tag{11}$$

$$y = (L^2 + a^2 + d^2 - 2ad\cos\varphi)^{0.5}\sin\left(\int_0^{\varphi}\frac{a(L^2 + (a - d\cos\xi)^2)^{0.5}}{L^2 + a^2 + d^2 - 2ad\cos\xi}d\xi\right), \tag{12}$$

$$\theta = \tan^{-1}((a - d\cos(\varphi))/L), \tag{13}$$

$$\psi = -\tan^{-1}(d\sin(\varphi)/(L/\cos(\theta))) + \int_0^{\varphi}\frac{a(L^2 + (a - d\cos\xi)^2)^{0.5}}{L^2 + a^2 + d^2 - 2ad\cos\xi}d\xi. \tag{14}$$

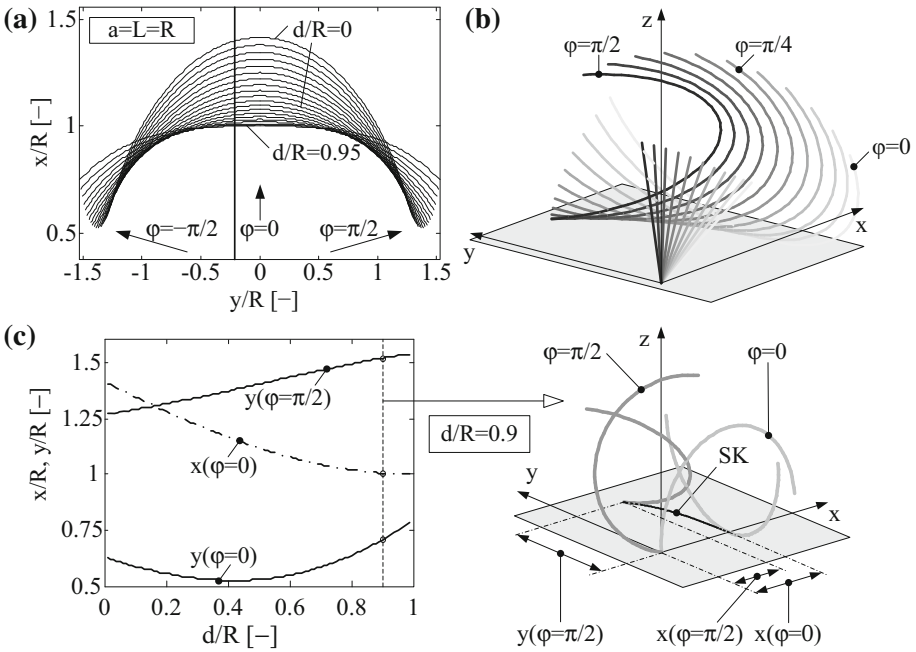

Fig. 3 Path of the contact point K on the ground in dependence of d ($a = L = R$) for two basic movement sequences ($\varphi = -\pi/2 \ldots \pi/2$) (**a**); rotation during a basic movement sequence (**b**) ($\varphi = 0 \rightarrow \pi/2$, gray $\rightarrow$ black, $d/R = 0.5$); and detailed results for the case $d/R = 0.9$

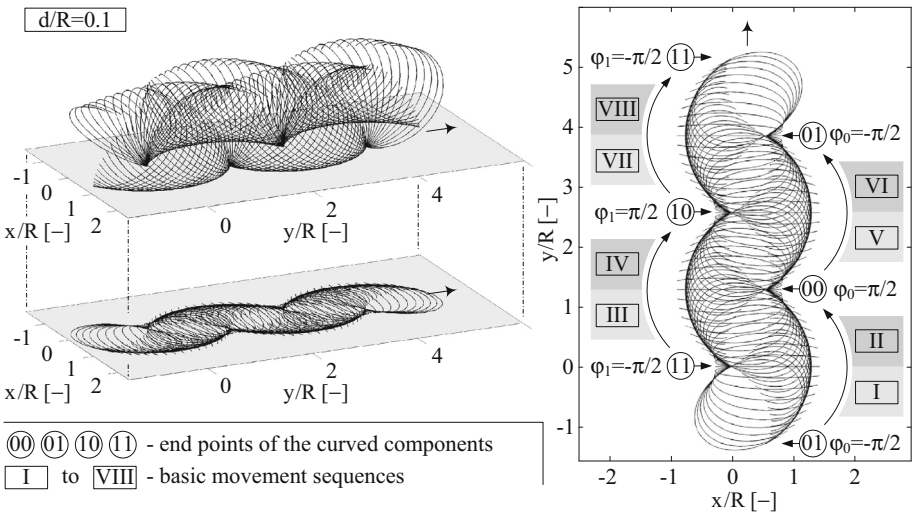

Fig. 4 Rolling locomotion of the system in the positive y-direction for eight basic movement sequences (I→VIII), ($d/R = 0.1$, displaying only the curved compressed members)

For the considered tensegrity system, the disc and the rod are both replaced with semicircular arcs of radius R ($\varphi_j = -\pi/2 \ldots \pi/2$, $a = L = R$). With the help of the above kinematic considerations, it can be seen that the geometric parameter d (see Fig. 1) plays an essential role with respect to the rolling locomotion of the system (Fig. 3). The maximum covered travel distance within a basic movement sequence can be achieved if $d \rightarrow R$.

During locomotion, rolling on both curved members takes place successively alternating (see Figs. 4 and 5 for the case of eight basic movement sequences (I→VIII)). With repeating these eight movement sequences, uniaxial locomotion of the system in the positive y-direction can be realized. The change of the rotation directions for both curved members leads to locomotion in the opposite direction.

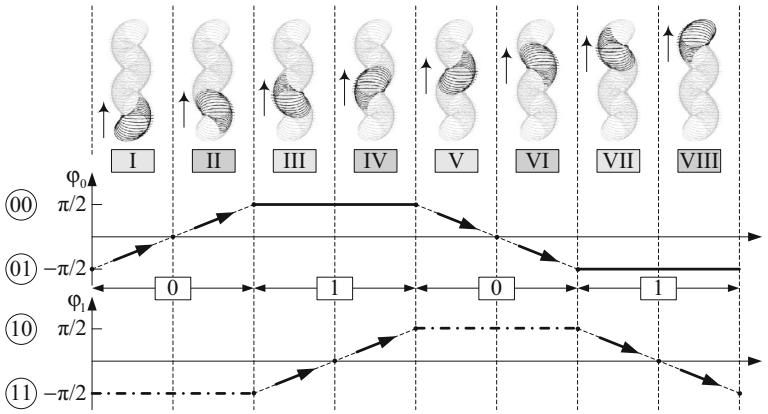

Fig. 5 Rolling locomotion of the system in the positive y-direction for eight basic movement sequences (I→VIII) – change of the angles φ_j ($d/R = 0.1$, displaying only the curved compressed members)

4 Dynamic system behavior for the basic movement sequence

The actuation of the system is carried out by changing the relative mass point positions $a_j(t)$ (see Fig. 1c). The goal is to determine the time-dependent position of the system $\varphi(t)$ for the basic movement sequence in dependence of the actuation parameters, characterized with $a_j(t)$. The description of the motion of the system is carried out with respect to the inertial x–y–z coordinate system. The system is considered as a system of mass points. The assumptions from Sect. 2 are still valid.

4.1 Equation of motion

The angular velocity and acceleration of the system can be expressed with

$$\vec{\omega} = \dot{\vec{\varphi}} + \dot{\vec{\psi}} + \dot{\vec{\theta}} = \dot{\varphi} \cdot \vec{C}_{d1}(\varphi), \tag{15}$$

$$\dot{\vec{\omega}} = \ddot{\varphi} \cdot \vec{C}_{d1}(\varphi) + \dot{\varphi}^2 \cdot \vec{C}_{d2}(\varphi), \tag{16}$$

where

$$\vec{C}_{d1}(\varphi) = \left\{ -\cos(\theta)\cos(\psi) + \frac{d\sin(\varphi)\sin(\psi)}{L((\tan(\theta))^2+1)}, -\cos(\theta)\sin(\psi) - \frac{d\sin(\varphi)\cos(\psi)}{L((\tan(\theta))^2+1)}, 0 \right\}^{\mathrm{T}}, \quad \vec{C}_{d2}(\varphi) = \dot{\vec{C}}_{d1}(\varphi) \cdot \dot{\varphi}^{-1}.$$

The position and velocity vectors of the mass points of the system are

$$\left(\vec{r}_{Aj}\right)^{\mathrm{T}} = \left\{ L \cdot (1-j) + j \cdot a_j \,,\ (1-j) \cdot (a_j - a) \,,\ (1-j) \cdot d \right\} \cdot [T(\varphi)] = \left(\vec{r}_{Aj,init}\right) \cdot [T(\varphi)], \tag{17}$$

$$\left(\dot{\vec{r}}_{Aj}\right)^{T} = \dot{\varphi} \cdot \left(\vec{r}^{\,*}_{Aj}\right)^{\mathrm{T}} + \left(\dot{\vec{r}}^{\,*}_{Aj,init}\right)^{\mathrm{T}}, \tag{18}$$

where

$$[T(\varphi)] = \begin{bmatrix} 1 & 0 & 0 \\ 0 & \cos(\varphi) & -\sin(\varphi) \\ 0 & \sin(\varphi) & \cos(\varphi) \end{bmatrix} \cdot \begin{bmatrix} \cos(\theta) & 0 & \sin(\theta) \\ 0 & 1 & 0 \\ -\sin(\theta) & 0 & \cos(\theta) \end{bmatrix} \cdot \begin{bmatrix} \cos(\psi) & \sin(\psi) & 0 \\ -\sin(\psi) & \cos(\psi) & 0 \\ 0 & 0 & 1 \end{bmatrix},$$

$$\left(\vec{r}^{\,*}_{Aj}\right)^{\mathrm{T}} = \left(\vec{r}_{Aj,init}\right) \cdot \dot{\varphi}^{-1} \cdot ([T(\varphi)])^{\cdot}, \quad \left(\dot{\vec{r}}^{\,*}_{Aj,init}\right)^{\mathrm{T}} = \left(\dot{\vec{r}}_{Aj,init}\right) \cdot [T(\varphi)].$$

The angular momentum and the moment of forces with respect to the origin O of the inertial coordinate system are (see Fig. 1c)

$$\vec{M}_{\mathrm{O}} = m \cdot \sum_{\mathrm{j}=0}^{1} \left(\vec{r}_{\mathrm{Aj}} \times \vec{g}\right) + \vec{r}_{\mathrm{K}} \times \vec{F}_{\mathrm{K}}, \vec{D}_{\mathrm{O}} = m \cdot \sum_{\mathrm{j}=0}^{1} \left(\vec{r}_{\mathrm{Aj}} \times \left(\vec{\omega} \times \vec{r}_{\mathrm{Aj}}\right)\right), \tag{19}$$

where $\vec{F}_{\mathrm{K}}$ is the contact force vector and $\vec{r}_{\mathrm{K}}$ the position vector with respect to the point K. Using the principle of angular momentum, the equation of motion of the model takes the form

$$\dot{\vec{D}}_{\mathrm{O}} - \vec{M}_{\mathrm{O}} = m \cdot \sum_{\mathrm{j}=0}^{1} \left(\dot{\vec{r}}_{\mathrm{Aj}} \times \left(\vec{\omega} \times \vec{r}_{\mathrm{Aj}}\right) + \vec{\mathrm{r}}_{\mathrm{Aj}} \times \left(\dot{\vec{\omega}} \times \vec{r}_{\mathrm{Aj}}\right) + \vec{r}_{\mathrm{Aj}} \times \left(\vec{\omega} \times \dot{\vec{r}}_{\mathrm{Aj}}\right) - \vec{r}_{\mathrm{Aj}} \times \vec{g}\right) - \vec{r}_{\mathrm{K}} \times \vec{F}_{\mathrm{K}} = \vec{0}. \tag{20}$$

Under the assumptions mentioned above, equation (20) can be rewritten as

$$\ddot{\varphi} + \dot{\varphi}^2 \cdot C_{\mathrm{dI}}(\varphi) + \dot{\varphi} \cdot C_{\mathrm{dII}}(\varphi) + C_{\mathrm{dIII}}(\varphi) = 0, \tag{21}$$

where

$$C_{\mathrm{dI}}(\varphi) = \frac{C_{\mathrm{d5}} C_{\mathrm{d2x}} + C_{\mathrm{d6}} C_{\mathrm{d2y}} + C_{\mathrm{d7}}}{C_{\mathrm{d5}} C_{\mathrm{d1x}} + C_{\mathrm{d6}} C_{\mathrm{d1y}}}, \quad C_{\mathrm{dII}}(\varphi) = \frac{C_{\mathrm{d8}}}{C_{\mathrm{d5}} C_{\mathrm{d1x}} + C_{\mathrm{d6}} C_{\mathrm{d1y}}}, \quad C_{\mathrm{dIII}}(\varphi) = \frac{C_{\mathrm{d9}}}{C_{\mathrm{d5}} C_{\mathrm{d1x}} + C_{\mathrm{d6}} C_{\mathrm{d1y}}},$$

with

$$\begin{aligned}
C_{\mathrm{d5}} &= \left(r_{\mathrm{A0y}}^2 + r_{\mathrm{A0z}}^2 + r_{\mathrm{A1y}}^2 + r_{\mathrm{A1z}}^2\right) - \frac{r_{\mathrm{Ky}}}{r_{\mathrm{Kx}}} \cdot \left(r_{\mathrm{A0x}} r_{\mathrm{A0y}} + r_{\mathrm{A1x}} r_{\mathrm{A1y}}\right) \\
C_{\mathrm{d6}} &= \frac{r_{\mathrm{Ky}}}{r_{\mathrm{Kx}}} \left(r_{\mathrm{A0x}}^2 + r_{\mathrm{A0z}}^2 + r_{\mathrm{A1x}}^2 + r_{\mathrm{A1z}}^2\right) - \left(r_{\mathrm{A0x}} r_{\mathrm{A0y}} + r_{\mathrm{A1x}} r_{\mathrm{A1y}}\right), \\
C_{\mathrm{d7}} &= \left(\sum_{\mathrm{j}=0}^{1} \left(\vec{r}_{\mathrm{Aj}}^{\,*} \times \left(\vec{C}_{\mathrm{d1}} \times \vec{r}_{\mathrm{Aj}}\right) + \vec{r}_{\mathrm{Aj}} \times \left(\vec{C}_{\mathrm{d1}} \times \vec{r}_{\mathrm{Aj}}^{\,*}\right)\right)\right) \cdot \left(\vec{e}_{\mathrm{x}} + \frac{r_{\mathrm{Ky}}}{r_{\mathrm{Kx}}} \cdot \vec{e}_{\mathrm{y}}\right), \\
C_{\mathrm{d8}} &= \left(\sum_{\mathrm{j}=0}^{1} \left(\dot{\vec{r}}_{\mathrm{Aj,init}}^{\,*} \times \left(\vec{C}_{\mathrm{d1}} \times \vec{r}_{\mathrm{Aj}}\right) + \vec{r}_{\mathrm{Aj}} \times \left(\vec{C}_{\mathrm{d1}} \times \dot{\vec{r}}_{\mathrm{Aj,init}}^{\,*}\right)\right)\right) \cdot \left(\vec{e}_{\mathrm{x}} + \frac{r_{\mathrm{Ky}}}{r_{\mathrm{Kx}}} \cdot \vec{e}_{\mathrm{y}}\right), \\
C_{\mathrm{d9}} &= -\left(\sum_{\mathrm{j}=0}^{1} \left(\vec{r}_{\mathrm{Aj}} \times \vec{g}\right)\right) \cdot \left(\vec{e}_{\mathrm{x}} + \frac{r_{\mathrm{Ky}}}{r_{\mathrm{Kx}}} \cdot \vec{e}_{\mathrm{y}}\right).
\end{aligned}$$

In the real case, during or after shifting of the mass points A_0 and A_1, a damped oscillation of the system with respect to the contact point O is to be expected. For simplifying reasons, this behavior can be approximated considering Stokes friction, with the friction coefficient k_{Sto}:

$$\ddot{\varphi} + \dot{\varphi}^2 \cdot C_{\mathrm{dI}}(\varphi) + \dot{\varphi} \cdot \left(C_{\mathrm{dII}}(\varphi) + k_{\mathrm{Sto}}\right) + C_{\mathrm{dIII}}(\varphi) = 0. \tag{22}$$

4.2 Simulations

In the simulations, the following position changes of the system are considered: $\varphi = 0 \rightarrow \pm\pi/2$ (initial conditions: $\varphi(t=0) = 0, \dot{\varphi}(t=0) = 0$) and $\varphi = \pm\pi/2 \rightarrow 0$ (initial conditions: $\varphi(t=0) = \pm\pi/2, \dot{\varphi}(t=0) = 0$). Model parameters are: $a = L = R = 80$ mm, $m = 25$ g, $d/R = 0.7$. Actuation parameters are the start and end times $(t_{\mathrm{j,start}}, t_{\mathrm{j,end}})$ of the actuation and the associated relative positions $(a_{\mathrm{j,start}}, a_{\mathrm{j,end}})$ of the mass points

$$a_{\mathrm{j}}(t) = \begin{cases} a_{\mathrm{j,start}} & \text{if } t < t_{\mathrm{j,start}} \\ a_{\mathrm{j,start}} + \left(a_{\mathrm{j,end}} - a_{\mathrm{j,start}}\right) \cdot \left(t - t_{\mathrm{j,start}}\right) / \left(t_{\mathrm{j,end}} - t_{\mathrm{j,start}}\right) & \text{if } t_{\mathrm{j,start}} \le t \le t_{\mathrm{j,end}} \\ a_{\mathrm{j,end}} & \text{if } t > t_{\mathrm{j,end}} \end{cases}. \tag{23}$$

Based on the simulations, the following results were found by varying the actuation parameters and the damping coefficient:

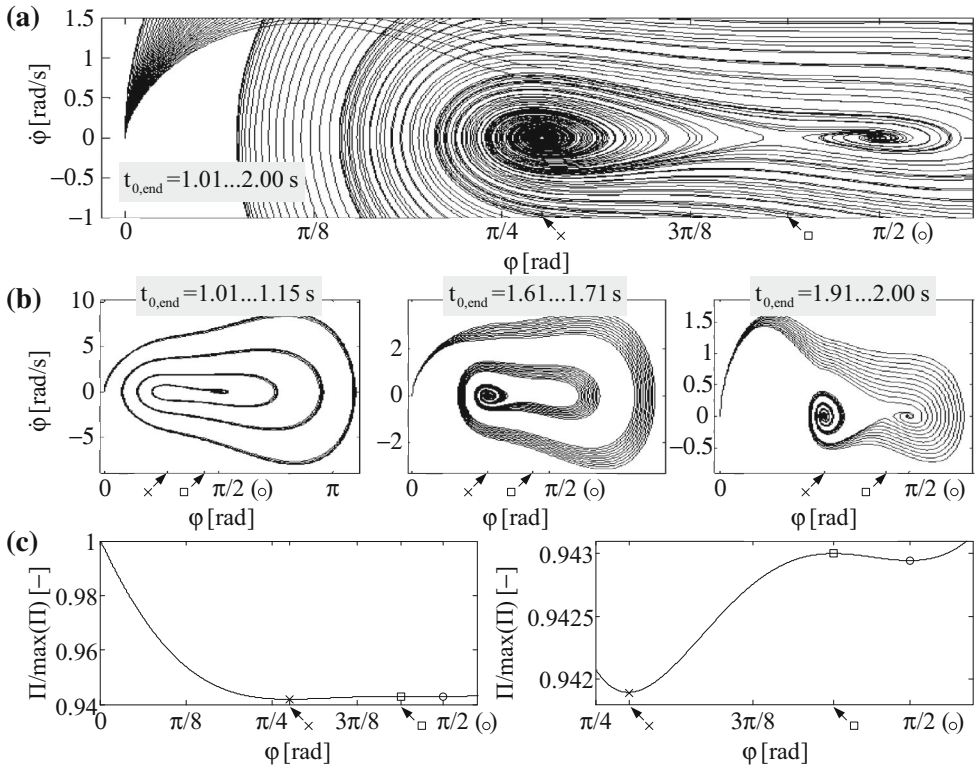

Fig. 6 Example 1 – influence of the speed of actuation of mass point A_0 on the system's equilibrium position after the actuation. Phase portraits for the considered speeds of actuation (**a**) and detailed views for selected subsets (**b**); normalized potential energy of the system for a_0=1.21R, $a_1 = 0.79R$ in dependence of φ (**c**); ($k_{\mathrm{Sto}} = 0.5$ Ns/mm, markers: x – $\varphi = 0.8689$, □ – φ=1.3813, o – $\varphi = \pi/2$)

- The change of the equilibrium position of the system from φ=0 to $\varphi = \pm\pi/2$ (basic sequence of movement) can be effected with the actuation of only one mass point (result 1).
- For specific cases, different equilibrium positions of the system can be achieved after the actuation, if the speed of actuation of the mass points is changed (for the case that several equilibrium positions of the system at given relative positions of the mass points after their actuation exist) (result 2).
- For specific cases, different equilibrium positions of the system can be achieved after the actuation, if the order of the actuated mass points is changed (for the case that several equilibrium positions of the system at given relative positions of the mass points after their actuation exist) (result 3).
- The vibration behavior of the system is essentially influenced by the speed of actuation of the mass points. Thus, an effective control algorithm can be determined to minimize the decay of oscillation of the system, so that the speed of the systems rolling movement can be maximized (result 4).

Regarding result 1, the case in which only mass point A_0 is moved (from $a_{0,\mathrm{start}} = 1R$ to $a_{0,\mathrm{end}} = 1.21R$) is considered. The relative position of mass point A_1 is constant: $a_{1,\mathrm{start}} = a_{1,\mathrm{end}} = 0.79R$. With respect to the initial conditions and selected initial positions of the mass points, the system is in stable equilibrium ($\varphi = 0$) at the beginning of the actuation. The dynamic system behavior is shown in Fig. 6 under varying the speed of movement of the mass point A_0, controlled by the parameter $t_{0,\mathrm{end}} = 1.01\ldots2$ s in 0.01 s steps ($t_{0,\mathrm{start}} = 1$ s). The results show that multiple ranges of the speed of actuation for mass point A_0 exist, for which at the end of the movement sequence the stable equilibrium position of the system at $\varphi = \pi/2$ can be realized (e.g. for $t_{0,\mathrm{end}} = 1.01\ldots1.15$ s). Thus, the actuation of only one mass point with an appropriate selected speed is sufficient to realize a basic movement sequence of the system. As the results further show, the system's equilibrium position at the end of movement varies in dependence of the speed of actuation, in accordance with result 2. Two stable equilibrium positions of the system are possible for the parameters $a_{0,\mathrm{end}}$=1.21R, $a_{1,\mathrm{end}} = 0.79R$: at φ =0.8689 and $\varphi = \pi/2$ (see markers x and o in Fig. 5).

Regarding result 2, a second case is considered in which both mass points are simultaneous actuated (from $a_{0,\mathrm{start}} = a_{1,\mathrm{start}} = R$ to $a_{0,\mathrm{end}} = 1.21R$, $a_{1,\mathrm{end}} = 0.79R$), with equal speeds of actuation. With respect to the

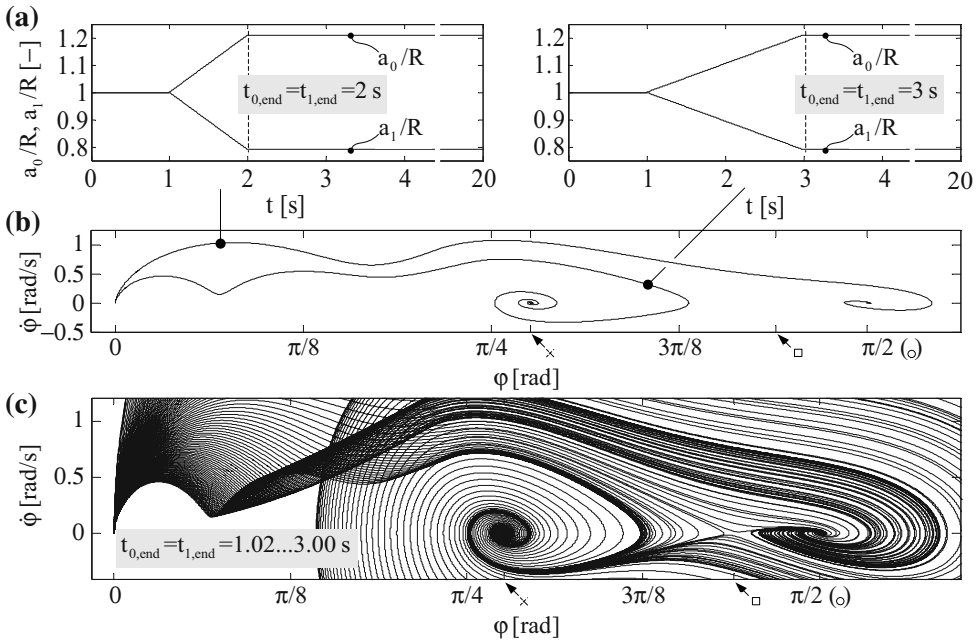

Fig. 7 Example 2 – influence of the speed of actuation on the system's equilibrium position after the actuation. Detailed view of two selected sets of actuation parameters over time (**a**) and corresponding phase portraits (**b**); phase portraits for the considered speeds of actuation (**c**) ($k_{Sto} = 1$ Ns/mm, markers: x – $\varphi = 0.8689$, □ – φ=1.3813, o – $\varphi = \pi/2$, see Fig. 6c)

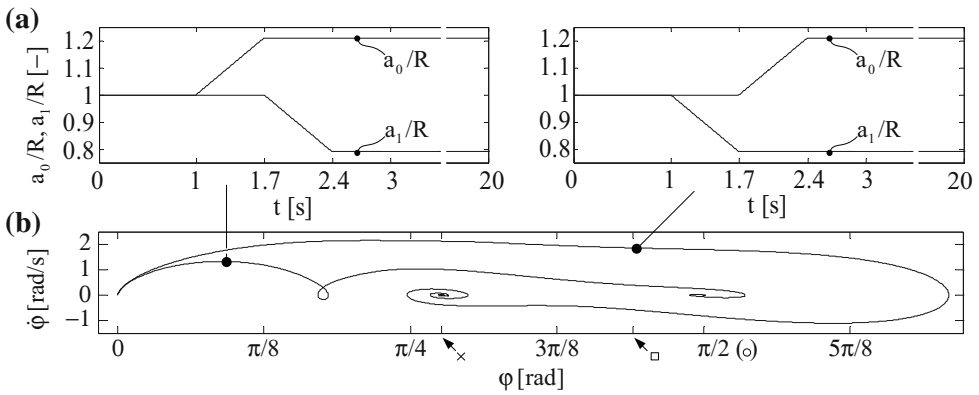

Fig. 8 Example 3 – influence of the order of the mass point actuation on the system's equilibrium position after the actuation. Two selected sets of actuation parameters over time (**a**) (left: $A_0 \rightarrow A_1$, right: $A_1 \rightarrow A_0$) and corresponding phase portraits (**b**) ($k_{Sto} = 1$ Ns/mm, markers: x – $\varphi = 0.8689$,□ – $\varphi = 1.3813$, o – $\varphi = \pi/2$, see Fig. 6c)

initial conditions and selected initial positions of the mass points, the system is in stable equilibrium ($\varphi = 0$) at the beginning of the actuation. Selected results for different speeds of actuation ($t_{0,\text{end}} = t_{1,\text{end}} = 1.02\ldots3$ s, step size: 0.02 s, $t_{0,\text{start}} = t_{1,\text{start}} = 1$ s) are depicted in Fig. 7. The equilibrium position of the system after the actuation depends in this case also on the applied actuation parameters.

Regarding result 3, an example is depicted in Fig. 8. As the results show, different equilibrium positions of the system after the actuation can be realized in dependence of the order of the actuated mass points ($A_0 \rightarrow A_1$: $\varphi = \pi/2$, $A_1 \rightarrow A_0$: $\varphi = 0.8689$).

The considered examples show that the motion of the system is essentially dependent on the type of actuation. Accordingly, the decay time of the oscillation (see result 4) and the maximum oscillation amplitude is decisively influenced by the actuation parameters. Due to the oscillation amplitudes, the use of curved members with $\max(|\varphi_j|) > \pi/2$ is required instead of semicircular arcs.

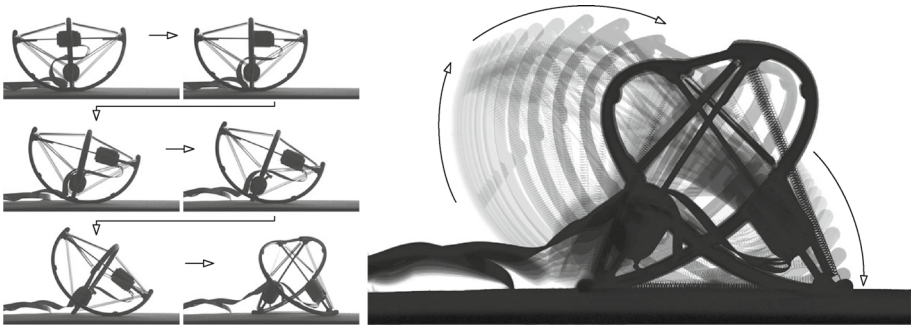

Fig. 9 Rolling motion of a preliminary prototype (*side view*) during a basic movement sequence (successively actuation of both internal masses)

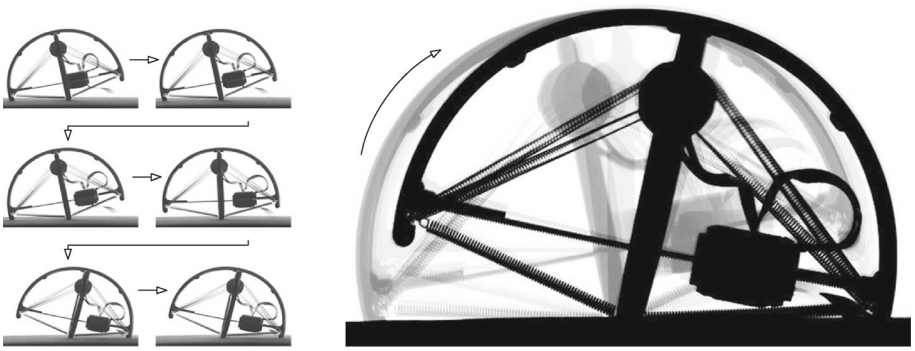

Fig. 10 Tip-over motion of a preliminary prototype (*side view*, actuation of only one internal mass)

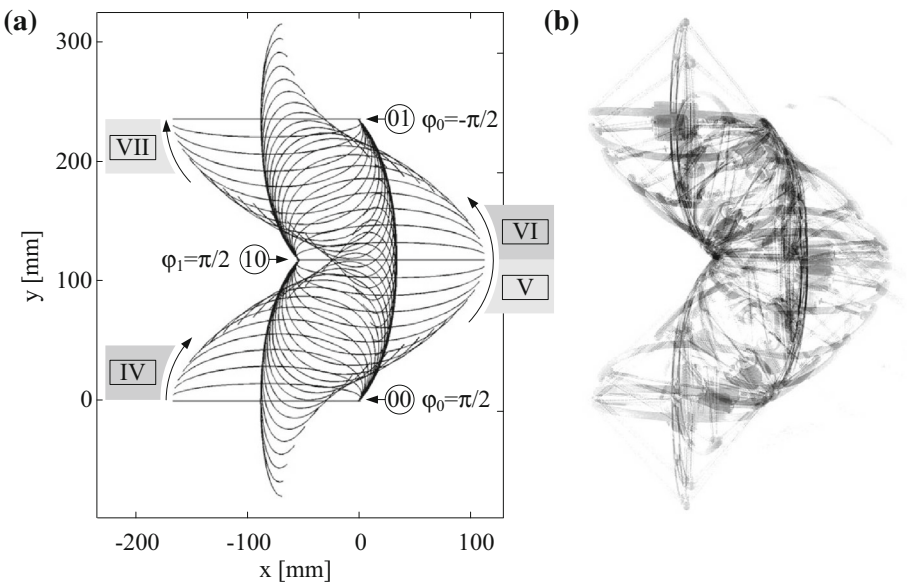

Fig. 11 Rolling motion of a preliminary prototype (top view) during four basic movement sequences (IV→VII see. Fig. 4, successively actuation of both internal masses). Theoretical (**a**) and experimental (**b**) data

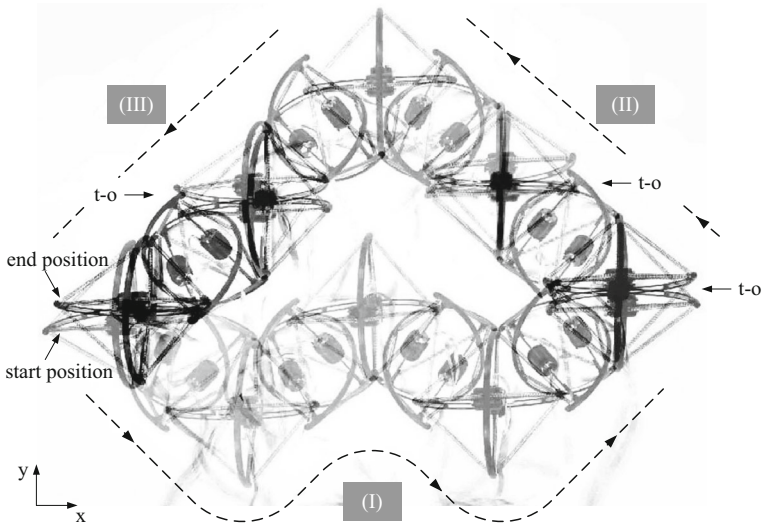

Fig. 12 Locomotion of a preliminary prototype in the x–y plane (*top view*) by using of pure rolling (I) and combined rolling and tip-over (t-o) movement sequences ((II) and (III))

4.3 Experimental tests

To verify the theoretical results, experimental tests on a preliminary prototype (see Fig. 1d, R = 85 mm, $d/R = 0.7705$, total mass: 168 g, internal masses: 2x56 g) were performed. With a high-speed camera, the system's movement for different actuation modes was recorded in different views (100 fps) and analyzed. As the results show, the prototype is able to realize the basic rolling movement sequence (see Fig. 9) and also tip-over movement sequence (see Fig. 10).

With repeating basic rolling movement sequences, rolling locomotion of the system without slipping can be achieved. Due to the high prestress of the robot's tensegrity structure, their elastic deformations during locomotion are negligible. Therefore, the kinematics of the prototype can be described quantitatively with the equations from Sect. 3 (see comparison of theoretical and experimental data in Fig. 11 and also in Fig.12). The main theoretical results from Sect. 4 were also verified qualitatively. Moderate quantitative differences are due to the simplified theoretical model.

To verify the locomotion performance of the preliminary prototype in the plane, rolling and tip-over movement sequences were executed repeatedly alternating. As the results show, the system is able to realize locomotion in the plane. To change the resulting locomotion direction, a tip-over movement sequence is needed.

5 Conclusions and future work

In this paper, basic dynamic properties of a rolling mobile robot, based on a non-conventional tensegrity structure, are presented. The actuation of the robot is realized with internal movement of two masses. It was shown that rolling locomotion can easily realized with tensegrity structures consisting of curved compressed members. Furthermore, the influence of mechanical parameters of the system's components and actuation parameters on the movement behavior is discussed.

Further work is focused on the extension of the mechanical model, including the masses of compressed and tensioned members. Also alternative actuation techniques, e.g. movement of the internal masses along the curved compressed members, will be considered.

Acknowledgements This work is supported by the Deutsche Forschungsgemeinschaft (DFG project BO4114/2-1).

References

1. Paul, C., Roberts, J.W., Lipson, H., Cuevas, F.J.V.: Gait production in a tensegrity based robot. In: Proceedings of ICAR '05, 12th international conference on advanced robotics, Seattle, pp 216–222 (2005)

2. Rieffel, J.A., Valero-Cuevas, F.J., Lipson, H.: Morphological communication: exploiting coupled dynamics in a complex mechanical structure to achieve locomotion. J. Roy. Soc. Interf. **7**, 613–621 (2010)
3. Koizumi, Y., Shibata, M., Hirai, S.: Rolling tensegrity driven by pneumatic soft actuators. In: Proceedings of IEEE international conference on robotics and automation, Saint Paul, pp 1988–1993 (2012)
4. Mirats Tur, J.M., Hernandez, S.: Tensegrity frameworks: Dynamic analysis review and open problems. Int. Journal of Mechanism and Machine Theory, 44(1), pp 1–18 (2009)
5. Skelton, R.E., De Oliveira, M.C.: Tensegrity Systems. Springer, Dordrecht (2009)
6. Khazanov, M., Jocque, J., Rieffel, J.: Evolution of Locomotion on a Physical Tensegrity Robot. In: Proceedings of the 14th international conference on the synthesis and simulation of living systems, New York, pp 232–238 (2014)
7. Caluwaerts, K., Despraz, J., Iscen, A., Sabelhaus, A.P., Bruce, J., Schrauwen, B., Sunspiral, V.: Design and control of compliant tensegrity robots through simulation and hardware validation. J. Roy. Soc. Interf. **11**, 20140520 (2014)
8. Böhm, V., Zeidis, I., Zimmermann, K.: An approach to the dynamics and control of a planar tensegrity structure with application in locomotion systems. Int. Journal of Dynamics and Control **3**(1), 41–49 (2015)
9. Kim, K., Agogino, A.K., Moon, D., Taneja, L., Toghyan, A., Dehghani, B., Sunspiral, V., Agogino, A.M.: Rapid Prototyping Design and Control of Tensegrity Soft Robot for Locomotion. In: Proceedings of IEEE international conference on robotics and biomimetics, Bali, pp 7–14 (2014)
10. Luo, A., Skelton, R.E., Liu, H., Liu, R., Guo, H., Wang, L.: Structure of the ball tensegrity robot. In: Proceedings of IEEE international conference on robotics and biomimetics, Bali, pp 1781–1786 (2014)
11. Sabelhaus, A.P., Bruce, J., Caluwaerts, K., Manovi, P., Firoozi, R.F., Dobi, S., Agogino, A.M., Sunspiral, V.: System design and locomotion of SUPERball, an untethered tensegrity robot. In: Proceedings of IEEE international conference on robotics and automation, Seattle, pp 2867–2873 (2015)
12. Böhm, V., Kaufhold, T., Zeidis, I., Zimmermann, K.: Dynamic analysis of the rolling locomotion of mobile robots based on tensegrity structures with two curved compressed components. In: Proceedings of the 13th Conference on Dynamical Systems - Theory and Applications, Łódź, pp 105–116 (2015)
13. Barber, G.T.: Structures composed of compression and tensile members. United States Patent, US **6868640**, B2 (2005)
14. Böhm, V., Jentzsch, A., Kaufhold, T., Schneider, F., Zimmermann, K.: An approach to compliant locomotion systems based on tensegrity structures. In: Proceedings of 56rd IWK – internationales wissenschaftliches kolloquium, Ilmenau (2011)
15. Böhm, V., Jentzsch, A., Kaufhold, T., Schneider, F., Becker, F., Zimmermann, K.: An approach to locomotion systems based on 3D tensegrity structures with a minimal number of struts. In: Proceedings of 7th german conference on robotics, München, pp 150–155 (2012)